

See discussions, stats, and author profiles for this publication at: <https://www.researchgate.net/publication/26650177>

Effect of Crystal Size and Surface Functionalization on the Cytotoxicity of Silicalite-1 Nanoparticles

ARTICLE in CHEMICAL RESEARCH IN TOXICOLOGY · AUGUST 2009

Impact Factor: 3.53 · DOI: 10.1021/tx900153k · Source: PubMed

CITATIONS

44

READS

45

5 AUTHORS, INCLUDING:



Jessica B Graham

Fred Hutchinson Cancer Research Center

11 PUBLICATIONS 127 CITATIONS

[SEE PROFILE](#)



Sarah C Larsen

University of Iowa

99 PUBLICATIONS 2,195 CITATIONS

[SEE PROFILE](#)



Aliasger K Salem

University of Iowa

121 PUBLICATIONS 2,201 CITATIONS

[SEE PROFILE](#)

Effect of Crystal Size and Surface Functionalization on the Cytotoxicity of Silicalite-1 Nanoparticles

Anton Petushkov,[†] Janjira Intra,[‡] Jessica B. Graham,[‡] Sarah C. Larsen,^{*,†} and Aliasger K. Salem^{*,‡}

Department of Chemistry, and Division of Pharmaceutics, College of Pharmacy, University of Iowa, Iowa City, Iowa 52242

Received April 28, 2009

In this report, we describe the synthesis and characterization of nanocrystalline silicalite (the purely siliceous form of the zeolite, ZSM-5) of defined crystal size and surface functionalization and determine the effect on the type and degree of cytotoxicity induced in two distinct model cell lines. The silicalite materials were characterized by powder X-ray diffraction, dynamic light scattering and ζ potential, solid state NMR, thermal gravimetric analysis, and nitrogen adsorption using the BET method to determine specific surface area. The silicalite samples were functionalized with amino, thiol, and carboxy groups and had crystal sizes of approximately 30, 150, and 500 nm. The cytotoxicities of the silicalite samples with different crystal sizes and different surface functional groups were investigated using human embryonic kidney 293 (HEK-293) cells and RAW264.7 macrophage cell lines. We used the lactic dehydrogenase release assay to measure damage to the cell membrane, the caspase 3/7 activity assay to measure key molecules involved in apoptosis, and the Annexin V-propidium iodide staining method to provide visual confirmation of the types of cell death induced. We have shown that the impact of size and surface functionalization of silicalite nanoparticles on cell toxicity and mechanism of cell death is cell type-dependent. Thirty nanometer silicalite nanoparticles were nontoxic in RAW264.7 cells relative to untreated controls but caused necrosis in HEK293 cells. Carboxy-functionalized 500 nm silicalite nanoparticles resulted in apoptosis and necrosis in RAW264.7 cells and predominantly activated apoptosis in HEK293 cells.

Introduction

The rapid growth and development in the synthesis of nanomaterials with carefully controlled properties, such as size and shape, surface area, and composition, has led to a burgeoning of potential applications for nanomaterials, in areas such as electronics, catalysis, optics, and medicine. Carbon-based nanomaterials (carbon nanotubes and buckyballs), semiconductor quantum dots (CdSe), metal nanoparticles and nanorods (gold, nickel, and platinum), and nanosized metal oxides (TiO_2) are important nanomaterials that have been widely studied. For example, metal nanoparticles and nanorods (gold, nickel and platinum) are being intensely investigated for applications in cancer detection (1, 2), imaging (1), and gene delivery (3–5). Porous nanomaterials (6–10), such as zeolites and mesoporous silica, have emerged as nanomaterials with new properties and many potential applications, in areas such as environmental catalysis (11), drug delivery (12, 13), and imaging (14–18).

The growing interest in nanomaterials and their potential applications in these important areas obviate the need to study the toxicity of nanomaterials prior to their widespread use in these far-reaching applications. The smaller size scale of nanoparticles may increase their toxicity or change the mechanism by which they induce toxicity. Toxicological data to date on “incidental” nanoparticles that are produced as a byproduct cannot necessarily be extrapolated to engineered nanoparticles

because they do not have the same size, composition, and surface properties (19). Studies of the toxicity of nanomaterials are further complicated by the fact that nanomaterials have size- and shape-dependent properties and are routinely prepared with specific surface coatings.

Zeolites are important commercial materials that are widely used in applications such as catalysis (20, 21), separations (22), water softening (22), and as bloodclotting (23) and imaging agents (16, 18, 24–26). Zeolites are porous, crystalline materials that have very large surface areas due to the internal surface area of the pores. Mesoporous silica is a related porous material that is amorphous and has larger pores than zeolites. Mesoporous silica has pores of >2 nm as compared to zeolite micropores of <2 nm. Mesoporous silica can be readily functionalized for applications in catalysis (27), imaging (17, 28, 29), and drug delivery (13, 30). Nanoscale zeolites are zeolites with crystal sizes of less than 100 nm, which have large surface areas due to appreciable internal and external surface areas (31, 32). The external surface area of nanoscale zeolites is up to an order of magnitude larger than the external surface area for micrometer-sized zeolites and provides an additional surface for reaction or functionalization (33–35). Functionalization of the external surface of nanoscale zeolites has been shown to be critical for applications in biomedicine, such as imaging (36) and drug delivery (12), and in the development of low dielectric materials (37) for the semiconductor industry.

Because of their numerous commercial applications, toxicity studies of zeolites (38) and crystalline silicas (39–45), such as quartz, have been reported in the literature. While studies of the natural zeolite, clinoptilolite, indicated that it is nontoxic

* To whom correspondence should be addressed. E-mail: sarah-larsen@uiowa.edu (S.C.L.) and aliasger-salem@uiowa.edu (A.K.S.).

[†] Department of Chemistry.

[‡] Division of Pharmaceutics, College of Pharmacy.

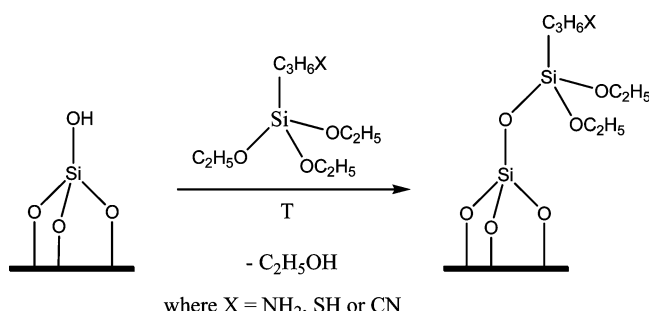


Figure 1. Reaction scheme depicting the reaction of the surface silanol groups with the organosilanes (APTES, MPTS, and CPTS) to form amino-, thiol-, and cyano-functionalized silicalite-1. The cyano-functionalized silicalite-1 was treated with sulfuric acid to form carboxy-functionalized silicalite-1.

and safe for human and veterinary use (8, 46), other studies have shown that crystalline silica materials may exhibit toxicity through silicosis, which is caused by inhalation of crystalline silica particles of respirable size. Extensive studies of crystalline silica materials such as quartz dusts have shown that physicochemical properties, such as particle size, shape, surface area, and surface chemistry, all impact toxicity. For example, in a study by Fubini and co-workers, the cytotoxicity of artificial crystalline silicas (differing size, morphology, and surface area) to macrophages was investigated (38). Macrophages were chosen because alveolar macrophages play a key role in silica-related diseases by clearing particles out of the lung or by causing chronic inflammation. Similar toxicity was observed for calcined versus uncalcined crystalline silicas, suggesting that the internal surface does not play a significant role in silica toxicity for these materials. The deposition of aluminum on the zeolite external surface was found to decrease toxicity (38).

Mesoporous silica, such as MCM-41, which in comparison to zeolites is amorphous, is being intensively investigated for biomedical applications (17, 47, 48). There have been several studies recently focused on the interaction of mesoporous silica materials with cells (49–52). Lin and co-workers investigated the effect of surface functionalization of MCM-41 on cellular uptake (52). Their study showed that the cellular uptake varied with surface functionality in that the ED₅₀ increased with decreasing ζ -potential. In a recent study by Asefa and co-workers, the toxicity of MCM-41 and functionalized MCM-41 showed that unfunctionalized MCM-41 was more toxic on a per particle basis toward human neuroblastoma (SK-N-SH) than aminopropyl- and mercaptopropyl-functionalized MCM-41 and that the most toxic mesoporous silica materials studied were those with the largest BET surface areas (50). Huang and co-workers determined that positively charged MCM-41 enhanced cellular uptake and that increased surface charge did not increase cytotoxicity (49). Another recent study suggested that mesoporous silica inhibited cellular respiration (51).

The focus of the work reported here is the cytotoxicity of silicalite with varying size and surface functionalization. In this study, silicalite-1, which has the MFI structure and is the purely siliceous form of the zeolite, ZSM-5, was synthesized with three different crystal sizes (~30, 150, and 500 nm) (31, 32). The silicalite external surface was functionalized by grafting of aminopropyl, mercaptopropyl, and carboxy functional groups onto the external zeolite surface as shown schematically in Figure 1. These functional groups were chosen so that the effect of surface charge on cytotoxicity could be systematically investigated. The silicalite materials were extensively characterized by powder X-ray diffraction (XRD), dynamic light scattering and ζ -potential, solid state NMR, thermal gravimetric

analysis (TGA), and nitrogen adsorption using the BET method to determine the specific surface area. The importance of careful characterization of nanomaterials for toxicity studies has been noted in the literature (19, 53–56).

The cytotoxicity of the silicalite samples with different crystal sizes and different surface functional groups was investigated using human embryonic kidney 293 (HEK-293) cells and the RAW264.7 macrophage cell lines. The rationale behind this selection of cell models is that the RAW264.7 cell line is a model macrophage cell line commonly used to represent the physiological scavengers of foreign nanoparticles. HEK293 cells were selected for evaluation in cytotoxicity studies because of their relevance and wide utility in the development of drug and gene delivery vehicles.

Cells can die by either of two major mechanisms: necrosis or apoptosis (57). Necrosis is the death of the cells through external damage, usually mediated via destruction of the plasma membrane or the biochemical supports of its integrity. Necrosis can occur in a matter of seconds. The other major form of cell death, apoptosis, is based on the concept of programmed cell death. Apoptosis is a much slower series of events than necrosis, requiring from a few hours to several days, depending on the initiator. The manifestations of apoptosis, both biochemical and morphological, are unique and are completely different from those of necrosis (58). In this study, we used the lactic dehydrogenase release (LDH) assay to measure damage to the cell membrane, the caspase 3/7 activity assay to measure key molecules involved in apoptosis, and the Annexin V-propidium iodide (PI) staining method to provide visual confirmation of the types of cell death induced relative to the size and surface functionalization of the silicalite nanoparticles.

Experimental Procedures

Silicalite-1 Preparation. Silicalite-1 was synthesized according to a well established procedure (1). Three batches of reaction mixture with the molar ratio of components TEOS:TPAOH:NaOH: H₂O as 25:9:0.16:495 were prepared. One batch was heated at 60 °C in an oil bath for 9 days, while the other two were heated at 165 °C in stainless steel autoclaves equipped with a PTFE liner for 46 and 56 h. The resultant suspensions were centrifuged at 14000 rpm for 20 min to separate the particles from the supernatant. The particles were then washed once with ethanol and twice with deionized water and dried at 90 °C overnight. All samples were calcined in air at 600 °C for 6 h to remove the organic template. Samples are labeled according to their crystal size estimated from BET. For example, 31 nm silicalite-1 will be referred to as silicalite-31.

Functionalization of Calcined Silicalite. Functionalization with amine groups was carried out by refluxing a mixture of 2 g of silicalite and 2 g of 3-aminopropyltriethoxysilane (APTES) in 60 mL of toluene for 4 h followed by centrifugation and washing of the silicalite powder with toluene. Functionalization with thiol groups was carried out by refluxing a mixture of 2 g of silicalite and 4 g of 3-mercaptopropyltriethoxysilane (MPTS) in 60 mL of toluene for 4 h followed by centrifugation and washing of the silicalite powder with toluene.

Functionalization with carboxypropyl groups was done in two steps. First, 2 g of silicalite was refluxed with 4 g of (3-ethoxysilyl)propionitrile (CPTS) in 60 mL of mesitylene overnight. The suspension was then centrifuged, and the crystals were washed with acetone. CPTS-functionalized silicalite was dried at 60 °C overnight. Then, the dry powder was suspended in 40 mL of 50% w/w sulfuric acid and refluxed for 6 h. The suspension was centrifuged, and the particles were washed with deionized water until the pH of the supernatant became neutral. Functionalized samples were dried in an oven at 60 °C overnight. Samples are labeled according to the functionalization and size. For example,

31 nm silicalite-1 that has been functionalized with APTES will be referred to as APTES-silicalite-31.

XRD and Nitrogen Adsorption. Both calcined and functionalized silicalite nanocrystals were characterized using powder XRD (Siemens D5000 X-ray diffractometer with Cu K α and nickel filter). The nitrogen adsorption isotherm (Nova 1200, Quantachrome) was measured to calculate specific surface area and particle size (in the case of as-synthesized crystals) for each sample. The specific surface obtained using the BET method on the as-synthesized samples, in which the template is still present in the pores, provides the external surface area, S_{ext} . As described previously in the literature (32), the BET external surface area can be used to calculate the silicalite crystal size assuming uniform cubic crystals by using the following equation:

$$S_{\text{ext}} = 3214/x$$

where S_{ext} is the external surface area in m^2/g and x is the silicalite-1 crystal size in nm. The total specific surface area is obtained using the BET method on the calcined silicalite samples.

Scanning Electron Microscopy (SEM). SEM images of the silicalite crystals were acquired using a Hitachi S-4800 scanning electron microscope. To prepare the sample for SEM, a drop of dilute colloidal solution of the sample in methanol was dropped onto the SEM sample stud surface, and the sample stud was then dried for 15 min at room temperature. Shortly before acquiring an SEM image, the sample was coated with gold.

ζ -Potential Measurements. The samples were prepared in the following way: 4 mg of sample was placed in disposable plastic tubes. Four milliliters of acetate (pH 4–6) and phosphate buffer (pH 6.2–8) solutions with matching ionic strengths was added to the silicalite powder, and the resulting suspensions were sonicated for 1 h (1510 Sonicator, Branson). The suspensions were allowed to settle overnight, and their pH (Corning pH meter 320) was checked prior to the ζ -potential measurements (Zetasizer Nano-ZS, Malvern Instruments).

Cell Culture. Human embryonic kidney 293 cells (HEK293) and macrophage cells (RAW264.7) were obtained from the American Type Culture Collection (Rockville, MD). The cells were maintained in Dulbecco's modified Eagle's medium (DMEM, Gibco) supplemented with 10% fetal bovine serum (Gibco), streptomycin at 100 $\mu\text{g}/\text{mL}$, penicillin at 100 U/mL, and 4 mM L-glutamine at 37 °C in a humidified 5% CO₂-containing atmosphere.

LDH Release Assay. The LDH activity from the incubation medium of cultured cells was assayed using the CytoTox 96 nonradioactive cytotoxicity assay kit from Promega Corp. (Madison, WI). HEK293 and RAW264.7 cells were seeded in V-bottom 96 cells/well at 1 \times 10⁴ and 1.5 \times 10⁴, respectively. Cells were treated with silicalite nanoparticles using a series of concentrations for 4 h at 37 °C. Fifty microliters of incubation medium was transferred into 96 well plates, mixed with 50 μL of reaction substrate mix, and incubated at room temperature for 30 min with light protection. Fifty microliters of stop solution was added into each well, and the optical density was measured at 490 nm using Spectramax plus³⁸⁴ Microplate Spectrophotometer (Molecular Device). Results were then normalized to untreated cells.

Caspase 3/7 Activity Assay. HEK293 and RAW264.7 cells were seeded in 75 cm² flasks in DMEM growth media at 37 °C with 5% CO₂ and allowed to reach 75–80% confluence. One \times 10⁴ cells for HEK293 and 1.5 \times 10⁴ RAW264.7 cells/well were plated in 100 μL volume per well in 96 well plates for 24 h. To measure caspase 3/7 activity, the Apo-ONEHomogenous Caspase-3/7 assay kit from Promega Corp. was used according to the manufacturer's protocol. Briefly, cells were incubated with silica nanoparticles at a concentration of 1 mg/mL for 4 h. After 4 h, 100 μL of reaction mixture (substrate in lysis buffer) was added and the fluorescence measured at 2 h using 485 (excitation) and 527 nm (emission) wavelengths (Spectra Max M5, Molecular Device). Untreated cells were used as negative controls, and cells treated with 1 μM staurosporine for 2 h were used as positive controls.

Annexin V-PI Staining. The Annexin V-PI staining method is commonly used to differentiate necrotic and apoptotic cells. For simultaneous detection of apoptotic and necrotic cell death, a costaining technique with fluorochrome-conjugated Annexin V, in tandem with the DNA-binding dye PI (Vybrant Apoptosis Kit #3, Molecular Probes) was used according to the manufacturer's instructions. Briefly, HEK293 and RAW264.7 cells were seeded in Lab-Tek II eight well chamber slides (Nalgene Nun Int., IL) at 2 \times 10⁵ cells/chamber using the same conditions as previous sets of experiments. Cells were incubated with different silicalite nanoparticles at 1 mg/mL for 4 h. After 4 h, the cells were washed in cold PBS. Cells were stained with Annexin V conjugate and PI. The images were taken using a Zeiss 510 NLO confocal laser-scanning microscope (Carl Zeiss Microscope Systems, Jena, Germany). Staining with Annexin-V identified apoptotic cells. Cells only stained with PI were identified as necrotic cells.

Statistical Analysis. The data are presented as means \pm standard errors. The statistical significance was determined using one-way analysis of variance (ANOVA) and the Tukey post-test, where $P < 0.05$ was considered significant. The data presented are representative of at least three repeats.

Results

Synthesis and Characterization of Silicalite-1 Nanoparticles with Three Different Crystal Sizes and Three Different Surface Functionalizations. Silicalite was synthesized in three different crystal sizes (approximately 30, 150, and 500 nm), and the samples were subsequently functionalized with amine (APTES), thiol (MPTS), and carboxylate (CPTS) functional groups as shown schematically in Figure 1. The silicalite crystal structure was confirmed by powder XRD. Representative X-ray powder patterns of the calcined and APTES-functionalized silicalite-31 samples (Figure S1, Supporting Information) reflect the MFI crystal structure and are very similar before and after functionalization, which indicates that the crystallinity of silicalite nanoparticles is retained during the surface functionalization. One exception was observed for the case of carboxy-functionalized silicalite with the smallest crystal size of 31 nm. To form carboxy-functionalized silicalite, the silicalite is first treated with CPTS to form the CPTS-silicalite followed by treatment with sulfuric acid to convert the cyano group to a carboxy group. However, for silicalite-31, after the sample was refluxed in sulfuric acid, a brown powder was recovered and the XRD pattern of the brown powder did not contain any characteristic silicalite reflections, which indicated the loss of crystallinity for this sample. When carboxy functionalization was carried out on 50 nm and larger silicalite particles, no loss of silicalite crystallinity was observed. It was concluded that the small size and high specific surface area, and therefore high surface free energy, potentially lead to instability of the smallest silicalite particles when they were refluxed in sulfuric acid.

Representative SEM images are shown in Figure 2 for (a) calcined silicalite-153 nm, (b) CPTS-silicalite-153, and (c) APTES-silicalite-153. The crystal morphology from the SEM images is approximately cubic and did not noticeably change when the sample was functionalized. The crystal size from SEM agrees with the crystal size obtained from the BET surface area as described below.

The BET specific surface area (S_{sp}) of the silicalite samples was measured to monitor the change of available surface area of calcined and functionalized samples (Table 1). The value of external S_{sp} was used to calculate the average crystal size formulas described previously (32) and in the Experimental Procedures. The silicalite samples had crystal sizes of approximately 30, 150, and 500 nm. Upon calcination, the organic template is removed from the silicalite pores, and the measured

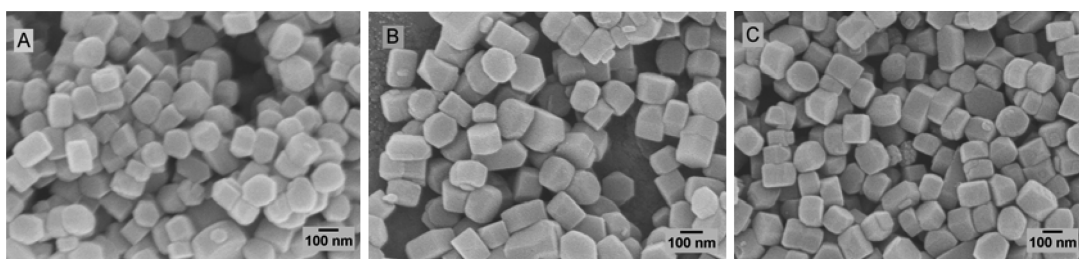


Figure 2. Representative SEM images of (A) calcined silicalite-153, (B) APTES-silicalite-153, and (C) CPTS-silicalite-153. Scale bars are 100 nm.

Table 1. Physicochemical Properties of Functionalized Silicalite Samples

| sample | average particle diameter ^a (nm) | S_{BET}^b [m ² /g calcined (as-synthesized)] | surface coverage ^c (mmol/g) | ζ -potential (mV at pH 7.4) ^d |
|----------------------|---|--|--|--|
| silicalite-31 | 31 | 340 (104) | — | -27.8 |
| APTES-silicalite-31 | 31 | 280 | 0.240 | 5.1 |
| MPTS-silicalite-31 | 31 | 313 | 0.176 | -11.1 |
| silicalite-153 | 153 | 298 (21) | — | -25.2 |
| APTES-silicalite-153 | 153 | 240 | 0.098 | -4.1 |
| MPTS-silicalite-153 | 153 | 275 | 0.069 | -16.2 |
| CPTS-silicalite-153 | 153 | 189 | 0.075 | -29.1 |
| silicalite-506 | 506 | 326 (6) | — | -31.1 |
| APTES-silicalite-506 | 506 | 269 | 0.066 | -11.7 |
| MPTS-silicalite-506 | 506 | 265 | 0.056 | -19.2 |
| CPTS-silicalite-506 | 506 | 178 | 0.077 | -43.9 |

^a Calculated from the external surface area of as-synthesized silicalite samples as determined from nitrogen adsorption and the BET method.

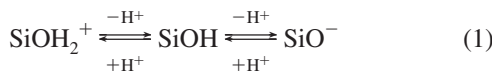
^b Specific surface area from nitrogen adsorption and the BET method.

^c Measured by TGA. ^d Calcined samples.

surface area is the sum of external and internal S_{sp} . Functionalization of silicalite nanoparticles results in a decrease in the total specific surface area. In the case of APTES-functionalized silicalite, the total S_{sp} decreased by up to 20% as compared to the calcined sample. A more pronounced decrease was observed for CPTS-silicalite samples (up to 45%). This has been observed previously for functionalized zeolites and is attributed to pore blocking by the organic groups that are grafted onto the surface possibly near the entrance to the zeolite pores (33).

Thermogravimetry was used to measure the functional group loading of the silicalite samples. A representative TGA curve is shown in Figure S4 of the Supporting Information, and the quantitative results are tabulated in Table 1. The TGA curves were similar for the different-sized silicalite samples. The amount of APTES functionalization in mmol/g silicalite increases from 0.066 mmol/g for APTES-silicalite-506 to 0.240 mmol/g for APTES-silicalite-31, which shows that the increased external surface area leads to increased capacity for surface functionalization (38).

The ζ -potential represents the surface charge of the particles in solution and varies with pH and ionic strength. The ζ -potentials for the calcined silicalite at pH 7.4 in phosphate buffer solution are listed in Table 1. The variation of the ζ -potential as a function of pH is shown in Figure S5 of the Supporting Information for silicalite with different functional groups. The ζ -potential shows similar trends with pH and functional groups for all of the silicalite sizes studied here. The ζ -potential of unfunctionalized silicalite reflects the protonation of surface hydroxyl groups according to the following equilibrium (eq 1).



The ζ -potential ranged from -28 to -31 mV for the different-sized silicalite samples, indicating that the surface silanol groups are deprotonated to SiO^- as indicated in eq 1. The ζ -potential is expected to change when the silicalite surface is functionalized with different organic groups.

For example, the ζ -potential for APTES-functionalized silicalite is governed by the following equilibrium (eq 2) involving the protonation of the surface amine groups.



Functionalization of silicalite with APTES leads to a marked positive shift of ζ -potential in comparison with calcined silicalite sample. The ζ -potential for APTES-silicalite-31 is more positive than the ζ -potential for the calcined silicalite. This reflects that the amine groups in the samples are protonated in this range of pH and is in agreement with alkylamine behavior in aqueous solutions. The ζ -potential for CPTS-silicalite-1 is governed by the following equilibrium (eq 3) involving the protonation of the surface carboxy groups.



Calculations of % ionization for propionic acid (which is expected to have a similar pK_a) show that about 10% of the acid is dissociated at pH 4 and almost completely dissociated at pH 8. Therefore, a smaller change in ζ -potential cannot be justified by the small dissociation constant. Another reasonable explanation is that reflux in sulfuric acid results in lower surface coverage with carboxy groups as some of them may be completely oxidized.

Silicalite samples with different sizes (\sim 30, 150, and 500 nm) were thoroughly characterized to ensure that the materials were crystalline and to determine the textural properties such as surface area and particle size. After functionalization with three different functional groups (amino, thiol, and carboxy), the silicalite-1 samples were further characterized by NMR (see the Supporting Information) and TGA to assess the functional group loading and molecular structure of the organic moiety and by ζ -potential to determine the stability and surface charge in phosphate buffer solution. The measurement of ζ -potential in phosphate buffer solution underscores the importance of characterization in the medium being used for the cytotoxicity study so that an understanding of the properties of the materials in the appropriate medium is obtained.

Toxicity of the Silicalite Nanoparticles Is Determined by Measuring Leakage of LDH and Caspase 3/7 Molecules. The silicalite nanoparticles of different sizes and different functionalization were tested using the LDH release assay (Figure 3)

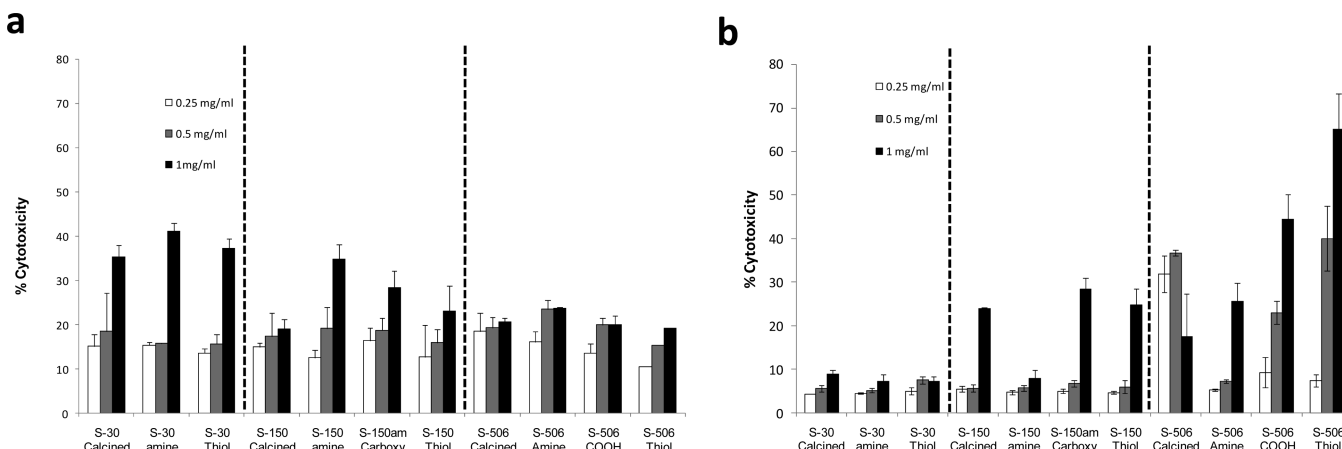


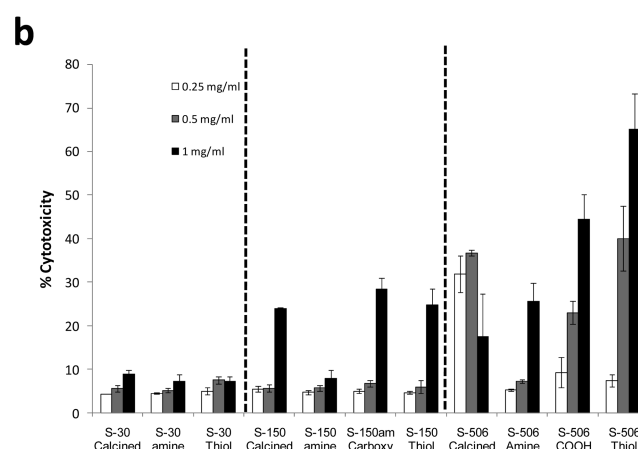
Figure 3. Cytotoxicity of calcined, amine-functionalized, thiol-functionalized, and carboxy-functionalized silicalite nanoparticles after 4 h of incubation in (a) HEK293 cells and (b) RAW264.7 macrophages as measured by the extent of LDH release. The extent of enzyme leakage is expressed as a percentage of the total activity (mean \pm SD of three separate experiments).

and the caspase 3/7 activity assay (Figure 4) to determine the degree of necrosis and apoptosis induced in HEK293 cells and RAW264.7 cells. These results were confirmed qualitatively using Annexin V-PI staining.

Toxicity as Measured by Leakage of LDH Is Dependent on Dose, Size, and Type of Surface Functionalization of Silicalite Nanoparticles and the Cell Type Being Tested. In HEK293 cells, low levels of LDH release were detected at concentrations of 0.25 and 0.5 mg/mL of silicalite nanoparticles (Figure 3a). Increasing the concentration of 30 nm silicalite nanoparticles incubated with the HEK293 cells increased LDH release activity by 2–3-fold ($P < 0.001$). While increasing the concentration of 30 nm silicalite nanoparticles incubated with HEK293 cells significantly increased LDH release activity, the surface functionalization of the silicalite nanoparticles with amine or thiol groups did not significantly change LDH release activity ($P > 0.05$). Functionalizing the surface of the 30 nm silicalite nanoparticles with amine or thiol groups had no significant effect on LDH release activity in RAW264.7 cells ($P > 0.05$). In RAW264.7 cells, increasing the dose of 30 nm silicalite nanoparticles from 0.25 to 1 mg/mL increased LDH release activity by 3–5%; however, relative to untreated controls, this was considered nontoxic (Figure 3b).

In HEK293 cells, the 150 nm calcined silicalite nanoparticles were nontoxic at all doses tested. In contrast, amine-, carboxy-, and thiol-functionalized silicalite nanoparticles all demonstrated dose-dependent toxicity with a 2–3-fold increase in LDH release activity when the dose was increased from 0.25 to 1 mg/mL ($P < 0.01$). Data from the LDH release activity assay showed that cell membrane damage was induced by nanoparticles functionalized in the following order: amine > carboxy > thiol > calcined.

In RAW264.7 cells, all 150 nm silicalite nanoparticles at or below 0.5 mg/mL dosing concentration were nontoxic. At 1 mg/mL dosing, however, calcined, carboxy-, and thiol-functionalized 150 nm silicalite nanoparticles all generated significant increases in LDH release activity that were approximately 4-fold higher than doses of 0.5 mg/mL ($P < 0.001$). The amine-functionalized 150 nm silicalite nanoparticles generated non-significant dose-dependent increases in LDH release activity in RAW264.7 cells. At a dosing of 1 mg/mL, the amine-functionalized silicalite nanoparticles were significantly less toxic than calcined, thiol-functionalized, and carboxy-functionalized silicalite nanoparticles ($P < 0.001$). This was only observed in the RAW264.7 cells ($P < 0.001$) and not the HEK293 cells ($P > 0.05$), indicating that reduced toxicity observed through amine functionalization is cell type-specific.



At 500 nm, the silicalite nanoparticles demonstrated dose-dependent toxicity in HEK293 cells, but these increases were small. Functionalization of the 500 nm silicalite nanoparticles did not significantly change the LDH release activity in HEK293 cells. In comparison, the functionalized 500 nm silicalite nanoparticles generated significant dose-dependent LDH release activity/toxicity in RAW264.7 cells that increased approximately 5–9-fold when the dose was increased from 0.25 to 1 mg/mL ($P < 0.001$). Functionalization of the silicalite nanoparticles had a significant impact on LDH release activity with thiol-functionalized silicalite nanoparticles generating the highest toxicity at 1 mg/mL dosing in RAW264.7 cells. Functionalization of the 500 nm silicalite nanoparticles increased toxicity in the following order thiol > carboxy > amine, and in contrast to HEK293 cells, these differences were significant ($P < 0.001$).

In HEK293 cells at 1 mg/mL dosing, the 30 nm silicalite nanoparticles generated the highest toxicity regardless of functionalization, while the 30 nm silicalite nanoparticles had no significant impact on LDH release activity in RAW264.7 cells. In contrast, the 500 nm silicalite nanoparticles at 1 mg/mL generated the highest LDH release activity in RAW264.7 cells, and the degree of toxicity was linked to the nature of the functionalization. These same 500 nm silicalite nanoparticles did not cause significant LDH release activity/toxicity in HEK293 cells regardless of the type of functionalization.

Toxicity as Measured by Caspase Activity Is Most Significant in Cell Lines Treated with Carboxy-Functionalized 500 nm Silicalite Nanoparticles. The results of the caspase activity assays are shown in Figure 4a for HEK293 and Figure 4b for RAW264.7. In HEK293 and RAW264.7 cells, 30 nm silicalite nanoparticles did not generate any significant caspase activity regardless of functionalization ($P > 0.05$). At a size of 150 nm, the silicalite nanoparticles that were calcined or functionalized with thiols did not generate significant increases in caspase activity relative to untreated controls in HEK293 or RAW264.7 cells ($P > 0.05$). Functionalization of the 500 nm silicalite nanoparticles did increase caspase activity with increases in the following order, carboxy > amine > calcined > thiol, for both HEK293 cells and RAW264.7 cell lines. The 500 nm silicalite nanoparticles generated the highest levels of caspase activity in HEK293 cells (except calcined 500 nm silicalite nanoparticles) and RAW264.7 cells in comparison to 150 nm silicalite nanoparticles and 30 nm silicalite nanoparticles regardless of functionalization. Functionalization of the 500 nm silicalite nanoparticles had a direct impact on caspase activity with the order of carboxy \gg amine $>$ thiol. The carboxy-functionalized

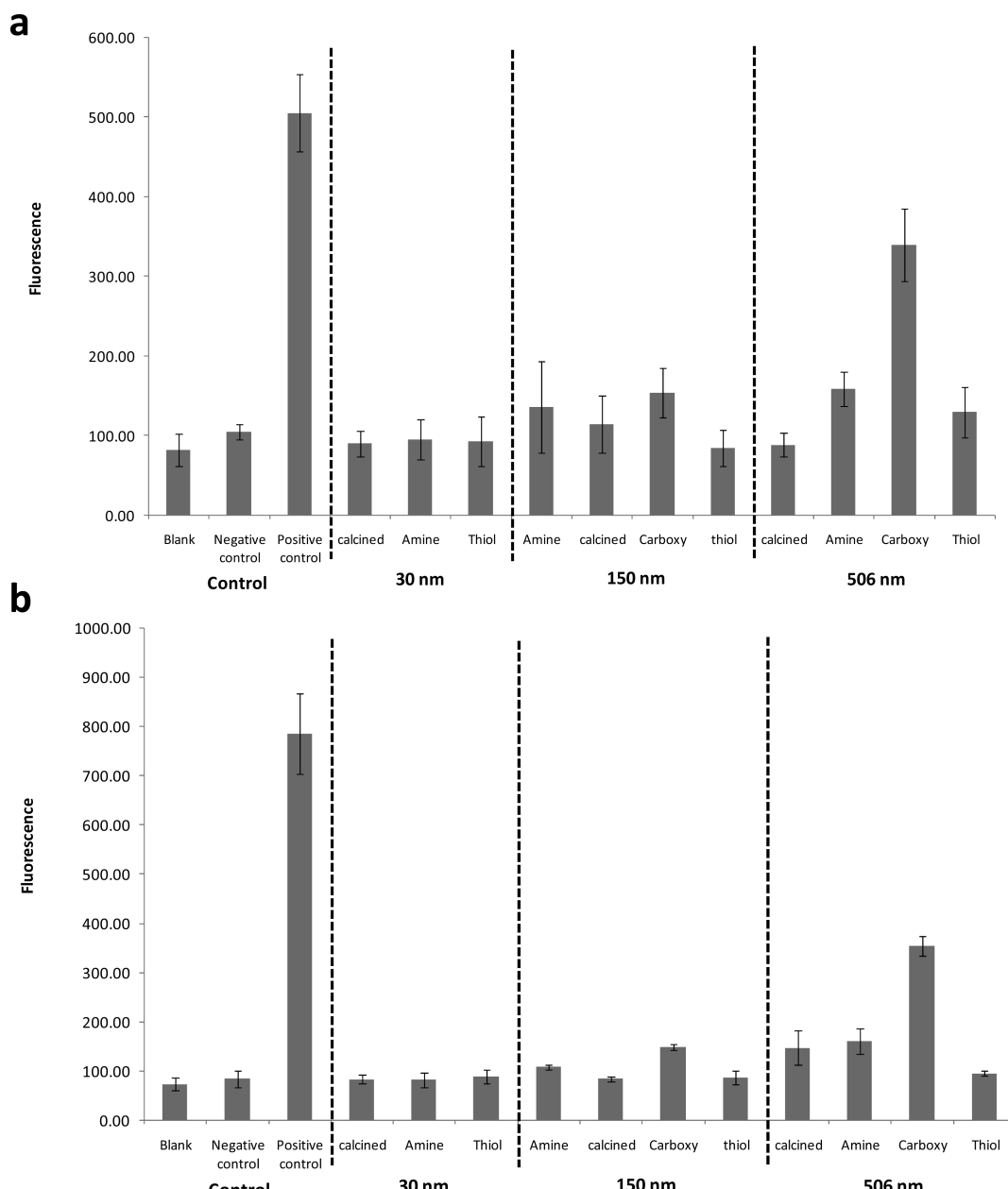


Figure 4. Cytotoxicity of calcined, amine-functionalized, thiol-functionalized, and carboxy-functionalized silicalite nanoparticles after 4 h of incubation in (a) HEK293 cells and (b) RAW264.7 macrophages as measured using the caspase 3/7 activity assay. Fluorescence is measured using 485 (excitation) and 527 nm (emission) wavelengths and presented as the mean \pm SD of three separate experiments.

500 nm silicalite nanoparticles generated significantly higher caspase activity than all other functionalizations and sizes of silicalite nanoparticles in HEK293 and RAW264.7 cells ($P < 0.001$). The LDH release assay and the caspase 3/7 assay were also carried out at different time points, and similar differences in the various groups were observed.

Annexin V-PI Staining Confirms Results from LDH Release Assay and Caspase 3/7 Activity Assays. Figure 5b shows HEK293 cells treated with 30 nm thiol-functionalized silicalite nanoparticles. Consistent with the results from the LDH release assay and the caspase 3/7 activity assay, the HEK293 cells are primarily stained with PI with limited Annexin-V fluorescent signals detected, suggesting that necrosis is the primary mechanism of cell death. Figure 5c shows HEK293 cells treated with carboxy-functionalized 500 nm silicalite nanoparticles. The majority of the HEK293 cells are double-stained with Annexin V and PI with apoptosis found to be the primary mechanism of cell death, and this is consistent with

the high caspase activity that was detected with this group. In RAW264.7 cells incubated with 500 nm carboxy-functionalized silicalite nanoparticles, in which both high LDH activity and caspase activity was induced, significant cell death was observed through necrosis and apoptosis (Figure 5d). Similar confocal fluorescent images provided visual confirmation of the type of cell death being induced by each of the various silicalite nanoparticles groups with different sizes and different surface functionalizations tested.

Discussion

Increasing evidence in the field of nanotoxicity is showing that the size, crystallinity, surface morphology, surface charge, and surface functional groups can have a significant impact on the degree of toxicity induced *in vitro* and *in vivo* (53–56, 59, 60). In this study, we complement existing data on toxicity induced by porous silica-based nanoparticles (38, 50, 51, 61) by showing,

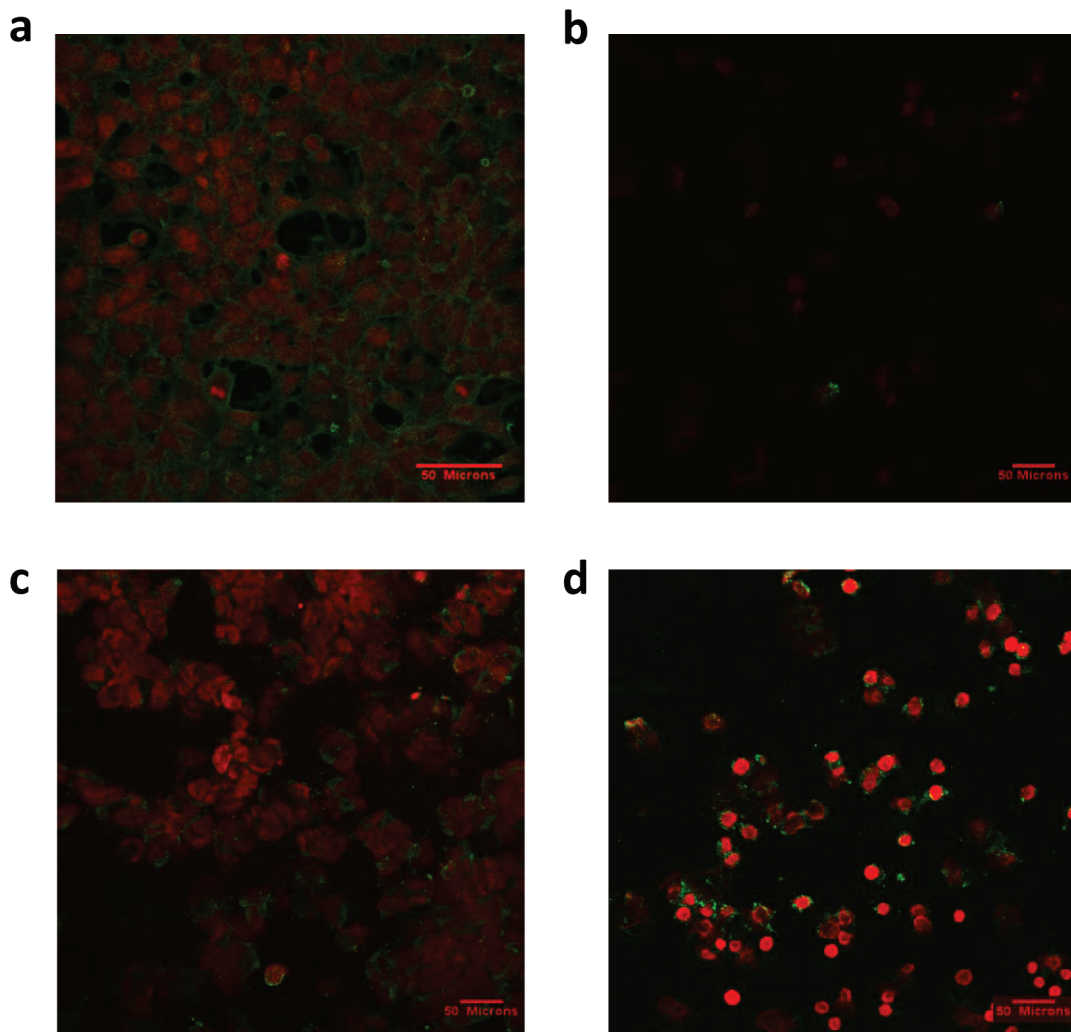


Figure 5. Representative confocal microscopy images of cells treated with Annexin V-PI staining. (a) Positive control of cells treated with 1 μ M staurosporine for 2 h, (b) HEK293 cells incubated with 30 nm silicalite nanoparticles functionalized with thiol groups for 4 h, (c) HEK293 cells incubated with 500 nm silicalite nanoparticles functionalized with carboxy groups for 4 h, and (d) RAW264.7 macrophages incubated with 500 nm silicalite nanoparticles functionalized with carboxy groups for 4 h.

for the first time, the effect of size and type of surface functionalization on apoptosis and necrosis-based toxicity. It is increasingly being recognized that a thorough physicochemical characterization of nanoparticles prior to testing for toxicity is essential to successfully correlate the properties of the nanoparticles to the toxicity profiles (54, 55, 62). In this study, we have carefully characterized the size, shape, surface morphology, surface charge, and surface functionalization of nanoscale silicalite using analytical tools such as NMR, TGA, powder XRD, nitrogen adsorption, and dynamic light scattering. In particular, the measurements of the size and surface charge were conducted in the buffer solutions that were used for the cytotoxicity assays.

To measure toxicity, we first measured LDH levels. The leakage of LDH from cells provides a direct measure of the damage/integrity to the cell membrane. At the highest concentrations tested for LDH activity, we then tested the silicalite nanoparticles with different functionalizations and different sizes for toxicity using the caspase 3/7 activity assay. Some of the key molecules involved in apoptosis are members of a family of cysteine aspartic acid-specific proteases called caspases. Caspases participate in a proteolytic cascade that leads to the programmed death of cells. Initiator caspases such as caspases 8 and 10 have an early role in the cascade, while effector caspases such as caspases 3, 6, and 7 are involved at later stages. As a result, measuring caspase 3/7 activity allows for a strong

correlation of the degree of apoptosis occurring in a cell population. The Apo-ONE Homogeneous Caspase-3/7 Assay works by providing cells with a substrate that fluoresces following cleavage by the activated caspases 3 and 7. The Annexin V-PI staining method was then used to provide visual confirmation of the type of cell death induced by the different functionalized silicalite nanoparticles. Annexin-V FITC is a 35.8 kDa protein that has a strong natural affinity for phosphatidylserine, a membrane phospholipid that, soon after apoptosis initiates, translocates from the inner to the outer surface of the cell plasma membrane. Cells with preserved membranes are impermeable to PI. However, PI enters those cells with a damaged membrane, staining the DNA red.

Effect of Dose, Particle Size, and Cell Type. The degree of LDH release induced by silicalite nanoparticles is dependent on dose and particle size, but the impact of the particle size is dependent on the cell type being tested. In HEK293 cells, an increase from 0.5 to 1 mg/mL for 30 and 150 nm silicalite nanoparticles significantly increased LDH release. An increase of 0.5 to 1 mg/mL for 500 nm nanoparticles did not significantly increase LDH levels in HEK293 cells. Surprisingly, and in contrast to the HEK293 cells, increasing the dose of 30 nm silicalite nanoparticles from 0.5 to 1 mg did not cause a significant increase in toxicity when incubated in RAW264.7 cells. However, increasing the dose of 150 and 500 nm silicalite

nanoparticles from 0.5 to 1 mg did cause a significant increase in toxicity when incubated in RAW264.7 cells. Increasing the dose of larger silicalite nanoparticles increased toxicity in RAW264.7 cells, while increasing the dose of smaller silicalite nanoparticles increased toxicity in HEK293 cells.

These results are most likely related to the biological characteristics of each of these cell lines. HEK293 cells, which are a hypotriloid human cell line derived from the kidney and commonly used for drug and gene delivery efficacy testing, will preferentially internalize particles that are less than 300 nm by clathrin-mediated endocytosis (63). Particles above the 250–300 nm cutoff for endocytosis including the 500 nm silicalite nanoparticles would likely have greater difficulty entering the cell by this route, and the toxicity of these particles even with increasing dose would therefore be expected to be reduced. In contrast, the RAW264.7 cells are a macrophage-like cell line that have a greater capacity to phagocytose much larger particles extending into the micrometer-size range. As such, 500 nm particles would be expected to be internalized more easily in RAW264.7 cells when compared to HEK293 cells, and this would account for the dose-dependent toxicity at higher particle sizes. Interestingly, a recent study by Thrall et al. has shown that changing the size of silica nanoparticles from 10 to 500 nm did not significantly change any of the 1009 gene sets they tested that were present in RAW264.7 cells. This suggests that it is not genotoxicity that is being affected by the size of the silicalite nanoparticles (64). Results are presented on a per mass basis, which is the most common approach used in nanoparticle drug delivery research and many other toxicity studies (5, 12, 30, 38, 39, 50, 59, 65–69).

Fubini and co-workers have shown that the surface area and aspect ratio of porosils in the 0.5–15 μm size range correlate with macrophage toxicity (38). These results showed that the porosil aspect ratio and external surface area correlated with cytotoxicity. An increase in external surface area led to an increase in the observed cytotoxicity of the monocyte-macrophage cell line (J774). Rodlike zeolite crystals also showed an increase in cytotoxicity with increasing aspect ratio. Because the RAW264.7 cell line is a macrophage cell line, the experiments reported here with silicalite and the RAW264.7 cell line can be best compared to the studies of Fubini and co-workers. However, the toxicity of silicalite does not correlate with the surface area. For example, 30 nm silicalite particles have the largest external surface area yet show markedly lower toxicity relative to the largest 500 nm silicalite particles. Our studies were conducted with zeolite particles in a much smaller size range (the lower limit in the Fubini study is our upper limit for crystal size), and thus, as discussed above, the endocytosis process may be quite different. In a related study on mesoporous silica, Asefa and co-workers found that the cytotoxicity was related to absorptive surface area, but the nature of the surface functional group could not be ruled out (50). A distinct difference between the mesoporous silica and the zeolitic materials is that the pore size of the mesoporous silica materials studied is significantly larger, suggesting that the internal surface could have a greater role in cytotoxicity because it is accessible to a wider range of biological molecules. These previous studies both suggest that the role of the zeolite surface area plays an important and complex role in determining the cytotoxicity of the materials.

Effect of Functionalization. In HEK293 cells, the dominant parameter effecting increased LDH release was dose and particle size regardless of surface functionalization. However, dose, particle size, and surface functionalization were linked to LDH release activity in RAW264.7 cells. Surface functionalization

did not change the degree of toxicity in RAW264.7 cells incubated with 30 nm silicalite nanoparticles but did change toxicity induced by the 153 and 500 nm silicalite nanoparticles. For example, the larger 500 nm silicalite nanoparticles showed dose-dependent increases in toxicity that increased with surface functionalization in the order of amine < carboxylic acid < thiol. The amine-functionalized silicalite exhibits the lowest toxicity for both the 153 and the 500 nm silicalite particles and the most positive ζ -potential, suggesting some correlation with surface charge. Thiol groups have been reported to inhibit NO production, which is also linked to S-nitrosoglutathione (GSNO) production (70–72). One potential reason that thiol-functionalized 500 nm silicalite nanoparticles trigger strong LDH release but not apoptosis may be related to interference with levels of S-nitrosoglutathione (GSNO) and nitric oxide (NO) production. When GSNO is depleted, toxicity is induced in macrophages that is predominantly caused by necrosis (70). This could account for the large LDH release but low caspase 3/7 activity observed in RAW264.7 cells when treated with thiol-functionalized 500 nm silicalite nanoparticles.

Carboxylic acid-functionalized 500 nm silicalite nanoparticles generated significantly higher levels of caspase 3/7 activity when compared to all other groups. Previous studies comparing quantum dots coated with either amine groups or carboxylic acid groups have shown that the quantum dots coated with COOH groups to be significantly more toxic. These particles stimulated significantly higher pro-inflammatory cytokines such as IL-6, IL-8, and IL-10 that have been reported to be correlated with immunotoxicity and apoptosis (73). In addition, other studies have shown that COOH-coated nanoparticles are efficiently taken up by cells such as macrophages (74). It is likely that COOH-coated silicalite nanoparticles generate the strongest reactive oxygen species (ROS) production, which has been reported to be correlated to high levels of caspase 3/7 activity and apoptosis (75). Studies on quartz dusts have shown that surface modification can dramatically influence the toxicity (44, 61). For example, quartz modified with aluminum lactate or polyvinylpyridine-N-oxide (PVNO) was significantly less toxic, and this was correlated to lower production of hydroxyl radicals when the modified quartz was exposed to hydrogen peroxide. Preliminary studies of the radical-generating ability of our silicalite samples in the presence of hydrogen peroxide do not show a clear correlation with toxicity. Future studies will focus on measuring the production of hydroxyl radical species, ROS, pro-inflammatory cytokines, NO production, and GSNO production to evaluate the role of oxidative stress, immunotoxicity, and GSNO/NO levels on the degree of apoptosis and necrosis triggered in cells.

Conclusions

In summary, the cytotoxicity of nanoscale silicalite is complex and depends on the particle size, surface functional group, and cell line used for the toxicity studies. The differences observed in toxicity based on cell type are most likely due to the different mechanisms for nanoparticle uptake by the HEK293 and RAW264.7 cell lines. The effect of surface functionalization on cytotoxicity also depends on the cell line. Smaller silicalite particles show dose-dependent toxicity in HEK293 cells that is not dependent on surface functionalization, and larger particles show dose-dependent toxicity in RAW264.7 cells that is dependent on functionalization. The mechanism for cell death was examined and was also found to depend on the cell line. Thiol-functionalized 500 nm silicalite nanoparticles predominantly cause toxicity by necrosis in RAW264.7 cells, while

COOH-functionalized 500 nm silicalite nanoparticles predominantly trigger apoptosis as measured by caspase 3/7 activity in HEK293 and RAW264.7 cells.

Acknowledgment. A.K.S. and S.C.L. acknowledge grant support from NSF NER (CMMI-0608977) and the Center for Health Effects and Environmental Contamination (CHEEC) at the University of Iowa.

Supporting Information Available: Additional experimental details and figures of representative powder XRD patterns, ^{29}Si MAS NMR, ^{13}C CPMAS NMR, TGA graph, and ζ -potential vs pH titration curves. This material is available free of charge via the Internet at <http://pubs.acs.org>.

References

- (1) Wang, H. F., Huff, T. B., Zweifel, D. A., He, W., Low, P. S., Wei, A., and Cheng, J. X. (2005) In vitro and in vivo two-photon luminescence imaging of single gold nanorods. *Proc. Natl. Acad. Sci. U.S.A.* **102**, 15752–15756.
- (2) El-Sayed, I. H., Huang, X. H., and El-Sayed, M. A. (2005) Surface plasmon resonance scattering and absorption of anti-EGFR antibody conjugated gold nanoparticles in cancer diagnostics: Applications in oral cancer. *Nano Lett.* **5**, 829–834.
- (3) Salem, A. K., Hung, C. F., Kim, T. W., Wu, T. C., Searson, P. C., and Leong, K. W. (2005) Multi-component nanorods for vaccination applications. *Nanotechnology* **16**, 484–487.
- (4) Salem, A. K., Chen, M., Hayden, J., Leong, K. W., and Searson, P. C. (2004) Directed assembly of multisegment Au/Pt/Au nanowires. *Nano Lett.* **4**, 1163–1165.
- (5) Salem, A. K., Searson, P. C., and Leong, K. W. (2003) Multifunctional nanorods for gene delivery. *Nat. Mater.* **2**, 668–671.
- (6) Kralj, M. (2003) Biomedical and environmental potential of nanoporous materials. *Period. Biol.* **105**, 99–107.
- (7) Kralj, M., and Pavelic, K. (2003) Medicine on a small scale. *EMBO Rep.* **4**, 1008–1012.
- (8) Pavelic, K., Hadsija, M., Bedrica, L., Pavelic, J., Dikic, I., Katic, M., Kralj, M., Bosnar, M., Kapitanovic, S., Poljak-Blazi, M., Krizanac, S., Stojkovic, R., Jurin, M., Subotic, B., and Colic, M. (2001) Natural Zeolite clinoptilolite: new adjuvant in anticancer therapy. *J. Mol. Med.* **78**, 708–720.
- (9) Tosheva, L., and Valtchev, V. P. (2005) Nanozeolites: Synthesis, crystallization mechanism, and applications. *Chem. Mater.* **17**, 2494–2513.
- (10) Larsen, S. C. (2007) Nanocrystalline zeolites and zeolite structures: Synthesis, characterization, and applications. *J. Phys. Chem. C* **111**, 18464–18474.
- (11) Li, G. H., Jones, C. A., Grassian, V. H., and Larsen, S. C. (2005) Selective catalytic reduction of NO_2 with urea in nanocrystalline NaY zeolite (Vol. 234, p 401, 2005). *J. Catal.* **235**, 431–431.
- (12) Pearce, M. E., Mai, H. Q., Lee, N., Larsen, S. C., and Salem, A. K. (2008) Silicalite nanoparticles that promote transgene expression. *Nanotechnology* **19**, 175103.
- (13) Trewyn, B. G., Giri, S., Slowing, I. I., and Lin, V. S. Y. (2007) Mesoporous silica nanoparticle based controlled release, drug delivery, and biosensor systems. *Chem. Commun.* 3236–3245.
- (14) Tsai, C. P., Hung, Y., Chou, Y. H., Huang, D. M., Hsiao, J. K., Chang, C., Chen, Y. C., and Mou, C. Y. (2008) High-contrast paramagnetic fluorescent mesoporous silica nanorods as a multifunctional cell-imaging probe. *Small* **4**, 186–191.
- (15) Matheoud, R., Secco, C., Ridone, S., Inglese, E., and Brambilla, M. (2008) The use of molecular sieves to simulate hot lesions in F-18-fluorodeoxyglucose - positron emission tomography imaging. *Phys. Med. Biol.* **53**, N137–N148.
- (16) Li, W. S., Li, Z. F., Jing, F. Y., Yang, X. G., Li, X. J., Pei, F. K., Wang, X. X., and Lei, H. (2007) Zeolites Mn^{2+} -NaY as oral gastrointestinal tract contrast agents in magnetic resonance imaging. *Acta Chim. Sin.* **65**, 2029–2033.
- (17) Lin, Y. S., Hung, Y., Su, J. K., Lee, R., Chang, C., Lin, M. L., and Mou, C. Y. (2004) Gadolinium(III)-incorporated nanosized mesoporous silica as potential magnetic resonance imaging contrast agents. *J. Phys. Chem. B* **108**, 15608–15611.
- (18) Balkus, K. J., and Shi, J. M. (1996) A study of suspending agents for gadolinium(III)-exchanged hectorite. An oral magnetic resonance imaging contrast agent. *Langmuir* **12**, 6277–6281.
- (19) Colvin, V. L. (2003) The potential environmental impact of engineered nanomaterials. *Nat. Biotechnol.* **21**, 1166–1170.
- (20) Li, G. H., Larsen, S. C., and Grassian, V. H. (2005) An FT-IR study of NO_2 reduction in nanocrystalline NaY zeolite: Effect of zeolite crystal size and adsorbed water. *Catal. Lett.* **103**, 23–32.
- (21) Li, G. H., Larsen, S. C., and Grassian, V. H. (2005) Catalytic reduction of NO_2 in nanocrystalline NaY zeolite. *J. Mol. Catal. A: Chem.* **227**, 25–35.
- (22) Breck, D. W. (1974) *Zeolite Molecular Sieves: Structure, Chemistry, and Use*. Wiley-Interscience, New York.
- (23) Galownia, J., Martin, J., and Davis, M. E. (2006) Aluminophosphate-based, microporous materials for blood clotting. *Microporous Mesoporous Mater.* **92**, 61–63.
- (24) Bresinska, I., and Balkus, K. J. (1994) Studies of Gd(III)-exchanged Y-type zeolites relevant to magnetic-resonance-imaging. *J. Phys. Chem.* **98**, 12989–12994.
- (25) Young, S. W., Qing, F., Rubin, D., Balkus, K. J., Engel, J. S., Lang, J., Dow, W. C., Mutch, J. D., and Miller, R. A. (1995) Gadolinium zeolite as an oral contrast agent for magnetic-resonance-imaging. *J. Magn. Reson. Imaging* **5**, 499–508.
- (26) Platas-Iglesias, C., Elst, L., Zhou, W., Muller, R. N., Geraldes, C., Maschmeyer, T., and Peters, J. A. (2002) Zeolite GdNaY nanoparticles with very high relaxivity for application as contrast reagents in magnetic resonance imaging. *Chem.—Eur. J.* **8**, 5121–5131.
- (27) Huh, S., Wiench, J. W., Trewyn, B. G., Song, S., Pruski, M., and Lin, V. S. Y. (2003) Tuning of particle morphology and pore properties in mesoporous silicas with multiple organic functional groups. *Chem. Commun.* 2364–2365.
- (28) Liang, M., Lu, J., Kovochich, M., Xia, T., Ruehm, S. G., Nel, A. E., Tamanoi, F., and Zink, J. I. (2008) Multifunctional inorganic nanoparticles for imaging, targeting, and drug delivery. *ACS Nano* **2**, 889–896.
- (29) Rieter, W. J., Kim, J. S., Taylor, K. M. L., An, H. Y., Lin, W. L., Tarrant, T., and Lin, W. B. (2007) Hybrid silica nanoparticles for multimodal Imaging. *Angew. Chem., Int. Ed.* **46**, 3680–3682.
- (30) Slowing, I. I., Trewyn, B. G., Giri, S., and Lin, V. S. Y. (2007) Mesoporous silica nanoparticles for drug delivery and biosensing applications. *Adv. Funct. Mater.* **17**, 1225–1236.
- (31) Song, W., Grassian, V. H., and Larsen, S. C. (2005) High yield method for nanocrystalline zeolite synthesis. *Chem. Commun.* 2951–2953.
- (32) Song, W., Justice, R. E., Jones, C. A., Grassian, V. H., and Larsen, S. C. (2004) Size-dependent properties of nanocrystalline silicalite synthesized with systematically varied crystal sizes. *Langmuir* **20**, 4696–4702.
- (33) Song, W., Woodworth, J. F., Grassian, V. H., and Larsen, S. C. (2005) Microscopic and macroscopic characterization of organosilane-functionalized nanocrystalline Nazsm-5. *Langmuir* **21**, 7009–7014.
- (34) Barquist, K., and Larsen, S. C. (2008) Chromate adsorption on amine-functionalized nanocrystalline silicalite-1. *Microporous Mesoporous Mater.* **116**, 365–369.
- (35) Zhan, B.-Z., White, M. A., and Lumsden, M. (2003) Bonding of organic amino, vinyl, and acryl groups to nanometer-sized NaX zeolite crystal surfaces. *Langmuir* **19**, 4205–4210.
- (36) Lerouge, F., Melnyk, O., Durand, J. O., Raehm, L., Berthault, P., Huber, G., Desvaux, H., Constantinesco, A., Choquet, P., Detour, J., and Smahi, M. (2009) Towards thrombosis-targeted zeolite nanoparticles for laser-polarized Xe-129 MRI. *J. Mater. Chem.* **19**, 379–386.
- (37) Lew, C. M., Li, Z. J., Li, S., Hwang, S. J., Liu, Y., Medina, D. I., Sun, M. W., Wang, J. L., Davis, M. E., and Yan, Y. S. (2008) Pure-silica-zeolite MFI and MEL low-dielectric-constant films with fluorogenic functionalization. *Adv. Funct. Mater.* **18**, 3454–3460.
- (38) Fenoglio, I., Croce, A., Di Renzo, F., Tiozzo, R., and Fubini, B. (2000) Pure-silica zeolites (porosils) as model solids for the evaluation of the physicochemical features determining silica toxicity to macrophages. *Chem. Res. Toxicol.* **13**, 489–500.
- (39) Fubini, B., Zanetti, G., Altilia, S., Tiozzo, R., Lison, D., and Saffiotti, U. (1999) Relationship between surface properties and cellular responses to crystalline silica: Studies with heat-treated cristobalite. *Chem. Res. Toxicol.* **12**, 737–745.
- (40) Fubini, B. (1997) Surface reactivity in the pathogenic response to particulates. *Environ. Health Perspect.* **105**, 1013–1020.
- (41) Fubini, B. (1998) Surface chemistry and quartz hazard. *Ann. Occup. Hyg.* **42**, 521–530.
- (42) Fubini, B., and Arean, C. O. (1999) Chemical aspects of the toxicity of inhaled mineral dusts. *Chem. Soc. Rev.* **28**, 373–381.
- (43) Elias, Z., Poirot, O., Daniere, M. C., Terzetti, F., Marande, A. M., Dzwigaj, S., Pezerat, H., Fenoglio, I., and Fubini, B. (2000) Cytotoxic and transforming effects of silica particles with different surface properties in Syrian hamster embryo (SHE) cells. *Toxicol. in Vitro* **14**, 409–422.
- (44) Giovine, M., Pozzolini, M., Fenoglio, I., Scarfi, S., Ghiazza, M., Benatti, U., and Fubini, B. (2002) Crystalline silica incubated in ascorbic acid acquires a higher cytotoxic potential. *Toxicol. Ind. Health* **18**, 249–255.

- (45) Donaldson, K., and Borm, P. J. A. (1998) The quartz hazard: A variable entity. *Ann. Occup. Hyg.* 42, 287–294.
- (46) Grce, M., and Pavelic, K. (2005) Antiviral properties of clinoptilolite. *Microporous Mesoporous Mater.* 79, 165–169.
- (47) Giri, S., Trewyn, B. G., Stellmacher, M. P., and Lin, V. S.-Y. (2005) Stimuli-responsive controlled-release delivery system based on mesoporous silica nanorods capped with magnetic nanoparticles. *Angew. Chem. Int. Ed.* 44, 5038–5044.
- (48) Radu, D. R., Lai, C.-Y., Jeftinija, K., Rowe, E. W., Jeftinija, S., and Lin, V. S.-Y. (2004) A polyamidoamine dendrimer-capped mesoporous silica nanosphere-based gene transfection reagent. *J. Am. Chem. Soc.* 126, 13216–13217.
- (49) Chung, T. H., Wu, S. H., Yao, M., Lu, C. W., Lin, Y. S., Hung, Y., Mou, C. Y., Chen, Y. C., and Huang, D. M. (2007) The effect of surface charge on the uptake and biological function of mesoporous silica nanoparticles 3T3-L1 cells and human mesenchymal stem cells. *Biomaterials* 28, 2959–2966.
- (50) Di Pasqua, A. J., Sharma, K. K., Shi, Y. L., Toms, B. B., Ouellette, W., Dabrowski, J. C., and Asefa, T. (2008) Cytotoxicity of mesoporous silica nanomaterials. *J. Inorg. Biochem.* 102, 1416–1423.
- (51) Tao, Z. M., Morrow, M. P., Asefa, T., Sharma, K. K., Duncan, C., Anan, A., Penefsky, H. S., Goodisman, J., and Souid, A. K. (2008) Mesoporous silica nanoparticles inhibit cellular respiration. *Nano Lett.* 8, 1517–1526.
- (52) Slowing, I., Trewyn, B. G., and Lin, V. S. Y. (2006) Effect of surface functionalization of MCM-41-type mesoporous silica nanoparticles on the endocytosis by human cancer cells. *J. Am. Chem. Soc.* 128, 14792–14793.
- (53) Maynard, A. D., Aitken, R., Butz, T., Colvin, V. L., Donaldson, K., Oberdorster, G., Philbert, M., Ryan, J., Seaton, A., Stone, V., Tinkle, S., Tran, L., Walker, N., and Warheit, D. (2006) Safe handling of nanotechnology. *Nature* 444, 267–269.
- (54) Sayes, C. M., Wahi, R., Kurian, P., Liu, Y., West, J., Ausman, K., Warheit, D., and Colvin, V. L. (2006) Correlating nanoscale titania structure with toxicity. *Toxicol. Sci.* 92, 174–185.
- (55) Lewinski, N., Colvin, V., and Drezek, R. (2008) Cytotoxicity of nanoparticles. *Small* 4, 26–49.
- (56) Warheit, D. (2008) How meaningful are the results of nanotoxicity studies in the absence of adequate material characterization? *Toxicol. Sci.* 101, 183–183.
- (57) Kanduc, D., Mittelman, A., Serpico, R., Sinigaglia, E., Sinha, A. A., Natale, C., Santacroce, R., Di Corcia, M. G., Lucchese, A., Dini, L., Pani, P., Santacroce, S., Simone, S., Bucci, R., and Farber, E. (2002) Cell death: Apoptosis versus necrosis (review). *Int. J. Oncol.* 21, 165–170.
- (58) Proskuryakov, S. Y., Gabai, V. L., Konoplyannikov, A. G., Zamulaeva, I. A., and Kolesnikova, A. I. (2005) Immunology of apoptosis and necrosis. *Biochemistry (Moscow)* 70, 1310–1320.
- (59) Lison, D., Thomassen, L. C. J., Rabolli, V., Gonzalez, L., Napierska, D., Seo, J. W., Kirsch-Volders, M., Hoet, P., Kirschhock, C. E. A., and Martens, J. A. (2008) Nominal and effective dosimetry of silica nanoparticles in cytotoxicity assays. *Toxicol. Sci.* 104, 155–162.
- (60) Oberdorster, G., Oberdorster, E., and Oberdorster, J. (2005) Nanotoxicology: An emerging discipline evolving from studies of ultrafine particles. *Environ. Health Perspect.* 113, 823–839.
- (61) Schins, R. P. F., Duffin, R., Hohr, D., Knaapen, A. M., Shi, T. M., Weishaupt, C., Stone, V., Donaldson, K., and Borm, P. J. A. (2002) Surface modification of quartz inhibits toxicity, particle uptake, and oxidative DNA damage in human lung epithelial cells. *Chem. Res. Toxicol.* 15, 1166–1173.
- (62) Marquis, B. J., Love, S. A., Braun, K. L., and Haynes, C. H. (2009) Analytical methods to assess nanoparticle toxicity. *Analyst* 134, 425–439.
- (63) Marsh, M., and McMahon, H. T. (1999) Cell biology—The structural era of endocytosis. *Science* 285, 215–220.
- (64) Waters, K. M., Masiello, L. M., Zangar, R. C., Zangar, R. C., Karin, N. J., Quesenberry, R. D., Bandyopadhyay, S., Teeguarden, J. G., Pounds, J. G., and Thrall, B. D. (2009) Macrophage responses to silica nanoparticles are highly conserved across particle sizes. *Toxicol. Sci.* 107, 553–569.
- (65) Intra, J., Glasgow, J. A., Mai, H. Q., and Salem, A. K. (2008) Pulsatile release of biomolecules from polydimethylsiloxane (PDMS) chips with hydrolytically degradable seals. *J. Controlled Release* 127, 280–287.
- (66) Intra, J., and Salem, A. K. (2008) Characterization of the transgene expression generated by branched and linear polyethylenimine-plasmid DNA nanoparticles in vitro and after intraperitoneal injection in vivo. *J. Controlled Release* 130, 129–138.
- (67) Zhang, X. Q., Dahle, C. E., Weiner, G. J., and Salem, A. K. (2007) A comparative study of the antigen-specific immune response induced by co-delivery of CpG ODN and antigen using fusion molecules or biodegradable microparticles. *J. Pharm. Sci.* 96, 3283–3292.
- (68) Zhang, X. Q., Intra, J., and Salem, A. K. (2007) Conjugation of polyamidoamine dendrimers on biodegradable microparticles for nonviral gene delivery. *Bioconjugate Chem.* 18, 2068–2076.
- (69) Zhang, X. Q., Intra, J., and Salem, A. K. (2008) Comparative study of poly (lactic-co-glycolic acid)-poly ethyleneimine-plasmid DNA microparticles prepared using double emulsion methods. *J. Microencapsulation* 25, 1–12.
- (70) Borutaite, V., and Brown, G. C. (2003) Nitric oxide induces apoptosis via hydrogen peroxide, but necrosis via energy and thiol depletion. *Free Radical Biol. Med.* 35, 1457–1468.
- (71) Kumar, K. S., Singh, V. K., Jackson, W., and Seed, T. M. (2003) Inhibition of LPS-induced nitric oxide production in RAW cells by radioprotective thiols. *Exp. Mol. Pathol.* 74, 68–73.
- (72) Zamora, R., Matthys, K. E., and Herman, A. G. (1997) The protective role of thiols against nitric oxide-mediated cytotoxicity in murine macrophage J774 cells. *Eur. J. Pharmacol.* 321, 87–96.
- (73) Ryman-Rasmussen, J. P., Riviere, J. E., and Monteiro-Riviere, N. A. (2007) Surface coatings determine cytotoxicity and irritation potential of quantum dot nanoparticles in epidermal keratinocytes. *J. Invest. Dermatol.* 127, 143–153.
- (74) Clift, M. J. D., Rothen-Rutishauser, B., Brown, D. M., Duffin, R., Donaldson, K., Proudfoot, L., Guy, K., and Stone, V. (2008) The impact of different nanoparticle surface chemistry and size on uptake and toxicity in a murine macrophage cell line. *Toxicol. Appl. Pharmacol.* 232, 418–427.
- (75) Park, E. J., and Park, K. (2009) Oxidative stress and pro-inflammatory responses induced by silica nanoparticles in vivo and in vitro. *Toxicol. Lett.* 184, 18–25.

TX900153K